



## Thermal and flammability properties of polypropylene/carbon nanotube nanocomposites<sup>☆</sup>

Takashi Kashiwagi<sup>a,\*</sup>, Eric Grulke<sup>b</sup>, Jenny Hilding<sup>b</sup>, Katrina Groth<sup>a</sup>, Richard Harris<sup>a</sup>, Kathryn Butler<sup>a</sup>, John Shields<sup>a</sup>, Semen Kharchenko<sup>c</sup>, Jack Douglas<sup>c</sup>

<sup>a</sup>Fire Research Division, NIST, Mail Stop 8665, Gaithersburg, MD 20899-8665, USA

<sup>b</sup>Advanced Carbon Materials Center, University of Kentucky, Lexington, KY 40506, USA

<sup>c</sup>Polymers Division, NIST, Gaithersburg, MD 20899, USA

Received 2 February 2004; received in revised form 29 March 2004; accepted 29 March 2004

### Abstract

The thermal and flammability properties of polypropylene/multi-walled carbon nanotube, (PP/MWNT) nanocomposites were measured with the MWNT content varied from 0.5 to 4% by mass. Dispersion of MWNTs in these nanocomposites was characterized by SEM and optical microscopy. Flammability properties were measured with a cone calorimeter in air and a gasification device in a nitrogen atmosphere. A significant reduction in the peak heat release rate was observed; the greatest reduction was obtained with a MWNT content of 1% by mass. Since the addition of carbon black powder to PP did not reduce the heat release rate as much as with the PP/MWNT nanocomposites, the size and shape of carbon particles appear to be important for effectively reducing the flammability of PP. The radiative ignition delay time of a nanocomposite having less than 2% by mass of MWNT was shorter than that of PP due to an increase in the radiation in-depth absorption coefficient by the addition of carbon nanotubes. The effects of residual iron particles and of defects in the MWNTs on the heat release rate of the nanocomposite were not significant. The flame retardant performance was achieved through the formation of a relatively uniform network-structured floccule layer covering the entire sample surface without any cracks or gaps. This layer re-emitted much of the incident radiation back into the gas phase from its hot surface and thus reduced the transmitted flux to the receding PP layers below it, slowing the PP pyrolysis rate. To gain insight into this phenomena, thermal conductivities of the nanocomposites were measured as a function of temperature while the thermal conductivity of the nanocomposite increases with an increase in MWNT content, the effect being particularly large above 160 °C, this increase is not as dramatic as the increase in electrical conductivity, however.

Published by Elsevier Ltd.

*Keywords:* Nanocomposite; Carbon nanotube; Polypropylene

### 1. Introduction

There is a high level of interest in using nanoscale reinforcing fillers for making polymeric nanocomposite materials with exceptional properties [1–3]. One such application is an improvement in flammability properties of polymers with nanoscale additives because one weak aspect of polymers is that they are combustible under certain conditions; these nanocomposites provide a possible alternative to conventional flame retardants. Nanocompo-

sites are particle-filled polymers where at least one dimension of the dispersed particle is on the nanometer scale. When all three dimensions are of the order of nanometers, we are dealing with true nanoparticles, such as spherical silica, having an aspect ratio of 1. With this type of nanoparticle (average diameter of 12 nm), the decreased flammability of a poly(methyl methacrylate) (PMMA) nanocomposite has been demonstrated [4]. Another type of nanocomposite is characterized by particles having only one dimension on a nanometer scale. In this case, the filler is present in the form of sheets/layers, such as layered silicate or graphite that are one to a few nanometers thick and hundreds to thousands of nanometers in the other two dimensions. At present, the most common approach for an improvement in flammability has been

<sup>☆</sup> This article is a US Government work and, as such, is in the public domain in the United States of America.

\* Corresponding author. Tel.: +1-301-9756699; fax: +1-301-9754052.  
E-mail address: [takashi.kashiwagi@nist.gov](mailto:takashi.kashiwagi@nist.gov) (T. Kashiwagi).

the use of layered silicates having large aspect ratios. The flame retardant effectiveness of polymer/clay nanocomposites based on various polymer resins has been demonstrated and several flame retardant mechanisms have been proposed [5–13].

When two dimensions are on the nanometer scale and the third is larger, forming an elongated structure, we speak of nanotubes. With this type of nanoparticle, significant increases in mechanical properties and specifically in electric conductivity were reported for polymer carbon nanotube nanocomposites at low content levels of the nanotubes [14–20]. However, previously published studies on the flammability of polymer carbon nanotube nanocomposites were rather limited. Two brief papers involving multi-walled carbon nanotubes (MWNT) were published showing significant flame retardant effectiveness of polypropylene (PP)/MWNT (1 and 2% by mass) nanocomposites [21] and demonstrating a small improvement in flammability properties of ethylene-vinyl acetate (EVA)/MWNT (2.5 and 5% by mass) nanocomposites [22]. A recent paper demonstrates the flame retardant effectiveness of PMMA/single-walled carbon nanotubes (1% by mass) nanocomposites [23]. Although these papers demonstrate flame retardant effectiveness of polymer carbon nanotube nanocomposites, the flame retardant mechanism has not been elucidated. The objective of this paper is to understand the flame retardant mechanism of PP/MWNT nanocomposites by measuring certain thermal characteristics.

## 2. Experimental

### 2.1. Materials

MWNTs were made using xylene as a carbon source and ferrocene as a catalyst at about 675 °C [24]. Composites were prepared by melt blending the MWNT-polypropylene mixture in a Haake PolyLab shear mixer.<sup>1</sup> The mixer temperature was raised to 180 °C, and polypropylene pellets (Grade 6331, Montell Polyolefins) were added with a mixer rpm of 20. The pellets melted in about 3 min, and the mixer torque approached a constant value in about 5 min. MWNTs were added at this time and the mixing was continued for 30 min. Carbon black (CB) and PP were compounded by melt processing conducted on a B and P Process Equipment and Systems twin-screw extruder (co-rotating, intermeshing, 25:1 L:D). Operating conditions were 36.7 rad/s (350 rpm) screw speed and 200 ± 3 °C barrel temperature for all zones except the feed (190 ± 3 °C). Carbon black powders (N299 and N762 Sid Richardson Carbon Co.) and resin pellets were gravimetrically fed (2.5 kg/h total

discharge rate, 60 s residence time) using Brabender Mass Loss feeders. The powder feeder was set-up to run as a fraction, based on desired carbon black mass fraction, of the pellet feeder discharge rate to accurately maintain the desired composition. All samples were compression molded at 190 °C under a pressure of 6 metric tons to make 75 mm diameter by 8 mm thick disks.

### 2.2. Sample characterization

The morphologies of the nanotubes in the melt blended sample and in the collected residues were evaluated using scanning electron microscopy (SEM; Hitachi 3200N) and energy dispersive scattering (EDS, Noran) for composition. PP was removed from unburned samples by heating them in excess 1,2,4 trichlorobenzene to 160 °C, at which point the PP crystallites melted and dissolved into the solvent. The nanotubes were recovered from the suspension by hot filtration and were dried. The nanotube morphology in the collected residues was investigated using SEM directly after dispersion in alcohol with ultra sonication.

A high precision hot stage (HCS 600) in conjunction with the stand-alone temperature controller (STC 200) from INSTEC, Inc. was used to facilitate collection of optical microscopy images of PP/MWNT nanocomposites in the melt. The images were taken in transmission mode with a 100 × Nikon objective lens mounted on the Ernst Leitz Wetzlar microscope when the temperature of the melt reached 200 °C. A SONY CCD camera (Model XC-77) with no additional magnification was used to record the images.

A Mattson Instruments Galaxy 7020 FT-IR was used to measure transmission characteristics of 200 μm thick, compression molded film samples from 700 to 4000 cm<sup>-1</sup> with a resolution of 1 cm<sup>-1</sup>. Thermal gravimetric analyses (TGA) were conducted using a TA Instruments SDT 2960 at 10 °C/min from 25 to 800 °C in nitrogen and in air. The samples (~5 mg) were placed in open ceramic pans. The standard uncertainty on sample mass measurement is ± 1%.

Thermal conductivity was measured using a Thermo-fluxer (SWO Polymertechnik GmbH) in the temperature range from 40 °C to about 270 °C. The measurement technique is based on the line-source method [25]. A bubble-free sample of the polymer melt was obtained, by repeatedly inserting then compressing small amounts of polymer into a cylindrical sample container (diameter of 0.98 cm with a length of 2.5 cm). The container was located in the center of a well-temperature-controlled oven. A thin probe containing a heater wire and a small thermocouple was inserted on the centerline of the molten sample. A small change in the probe temperature (2–5 °C) after the start of power output from the probe heater was recorded and thermal conductivity was calculated from this temperature change within the first 10 s. The estimated uncertainty in the measured thermal conductivity is ± 10%.

<sup>1</sup> Certain commercial equipment, instruments, materials, services or companies are identified in this paper in order to specify adequately the experimental procedure. This in no way implies endorsement or recommendation by NIST.

### 2.3. Flammability property measurement

A cone calorimeter built by NIST was used to measure ignition characteristics, heat release rate, and sample mass loss rate according to ASME E1354/ISO 5660. An external radiant heat flux of  $50 \text{ kW/m}^2$  was applied. All of the samples were measured in the horizontal position and wrapped with thin aluminum foil except for the irradiated sample surface. The standard uncertainty of the measured heat release rate is  $\pm 10\%$ .

A radiant gasification apparatus, somewhat similar to a cone calorimeter, was designed and constructed at NIST to study the gasification processes of samples by measuring mass loss rate and temperatures of the sample exposed to a fire-like heat flux in a nitrogen atmosphere (no burning). The apparatus consists of a stainless-steel cylindrical chamber that is 1.70 m tall and 0.61 m in diameter. In order to maintain a negligible background heat flux, the interior walls of the chamber are painted black and the chamber walls are water-cooled to  $25^\circ\text{C}$ . All experiments were conducted at  $50 \text{ kW/m}^2$ . The unique nature of this device is threefold: (1) observation and results obtained from it are only based on the condensed phase processes due to the absence of any gas phase oxidation reactions and processes; (2) it enables visual observations of gasification behavior of a sample using a video camera under a radiant flux similar to that of a fire without any interference from a flame; (3) the external flux to the sample surface is well-defined and nearly constant over the duration of an entire experiment (and over the spatial extent of the sample surface) due to the absence of heat feedback from a flame. A more detailed discussion of the apparatus is given in our previous study [26]; the standard uncertainty of the measured mass loss is  $\pm 10\%$ .

## 3. Results and discussion

### 3.1. Sample morphology

The distribution of the nanotubes in the sample was examined by two different methods and magnifications. One used a scanning electron microscopy (SEM). A SEM picture of the recovered MWNTs from the unburned PP/MWNT (4% mass) sample is shown in Fig. 1. Although it shows well dispersed MWNTs *implying* good dispersion in the PP/MWNT nanocomposite, more direct observations and larger observation areas of the dispersion of MWNTs in the PP/MWNT samples are preferred. The second method used optical microscopy; an image of the unburned PP/MWNT(1%) is shown in Fig. 2. It shows globally well-dispersed nanotubes in PP at large scales and a wide range of diameters and lengths of nanotubes as shown in Fig. 1.

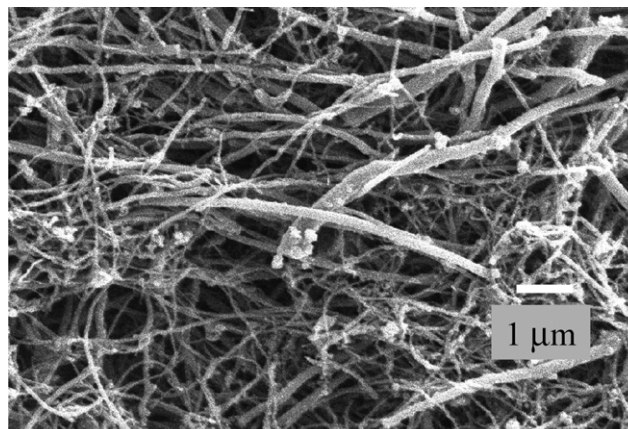


Fig. 1. SEM picture of MWNT dispersion in the PP/MWNT(4%) nanocomposite after solvent removal of PP.

### 3.2. Effects of residual iron and defects in MWNTs on flammability properties

The thermal oxidation stability of MWNT is significantly affected by defects (vacancies, kinks, dislocations, edges,...) and residual iron particles in the MWNTs [27, 28]. MWNTs used in the PP/MWNT nanocomposites contain 7.1% by mass of iron particles which are formed from ferrocene used as a catalyst to make the MWNTs [29]. The iron particles are encapsulated at various locations inside the nanotubes, and also as nanospheres near the nanotube tips. The nanotube tips are visible in Fig. 1 as the nodules at the end of some of the tubes. Nanoparticulate iron is pyrophoric, and could reduce the thermal oxidative stability of MWNT, as well as acting as a catalyst during the oxidative degradation of the PP/MWNT nanocomposites. Iron particles could form iron oxides during thermal degradation and iron oxides have been used as flame retardant additives to various polymers [30,31]. Furthermore, it was reported that radical trapping by the iron within clay enhanced the thermal stability of polystyrene (PS) in

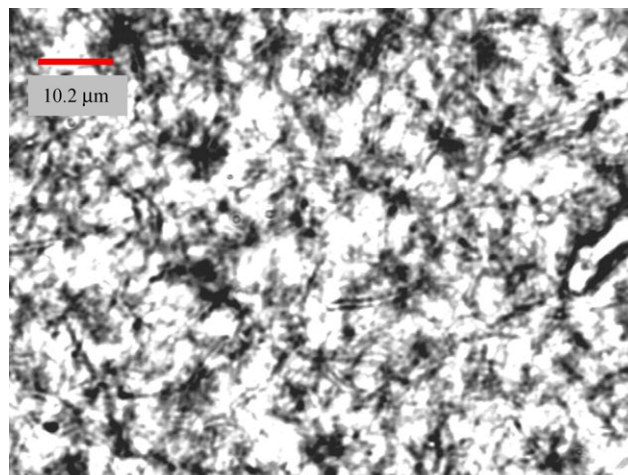


Fig. 2. Optical microscopy image of MWNT/PP(1%) nanocomposite in the melt.

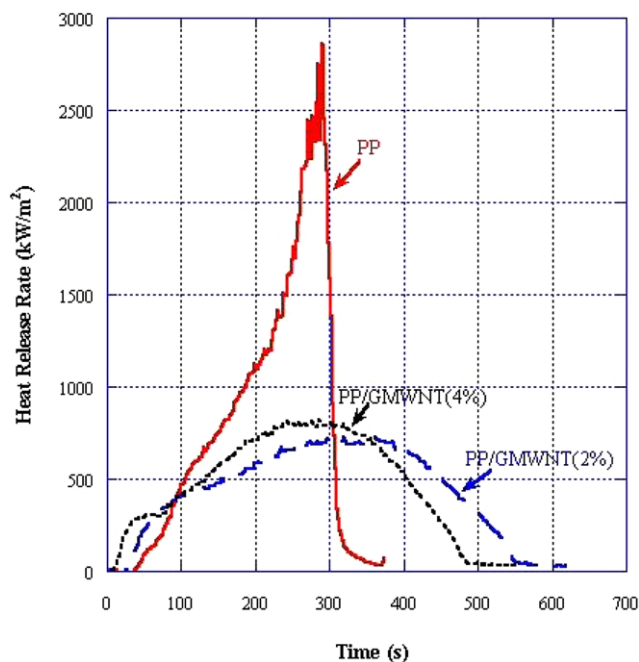


Fig. 3. Effects of addition of graphitized MWNTs on heat release rates of PP/GMWNT nanocomposites at  $50 \text{ kW/m}^2$ .

PS–clay nanocomposites [9]. However, the same study found that iron did not affect the thermal stability of PS in PS–iron containing graphite nanocomposites. Since the iron particles are inside and at the ends of the MWNT, their contact with PP chains would be minimal and would not occur until the walls of the nanotube tip were catalytically degraded. If this were so, the role of iron particles in MWNT might not be important for the thermal stability of the PP/MWNT nanocomposite. However, at present, the role of the iron particles and also the defects in MWNT in the flammability properties of the PP/MWNT nanocomposite is not known. Iron particles and the MWNT defects can be eliminated by annealing the MWNTs at a high temperature to make ‘graphitized’ MWNTs [28,29]; they are designated as GMWNTs and the nanocomposite with PP is designated as PP/GMWNT. The PP/GMWNT samples were made by

the same preparation as the PP/MWNT samples described in Section 2.1. An optical microscopy image of the unburned PP/GMWNT(1%) shows globally well-dispersed graphitized tubes in PP. The heat release rate curves of the PP/GMWNT samples are shown in Fig. 3. These results exhibit essentially the same as the heat release rate curves of PP/MWNT which were published in our previous study [21]. Thus, residual iron particles and the defects in MWNTs do not have significant effects on heat release rate of the PP/MWNT nanocomposite samples. However, strong glowing combustion (smoldering) of the sample residues (PP/MWNT with iron) was observed after flaming combustion was over during the cone calorimeter tests (Smoldering was not observed with the residue of PP/GMWNT under the same condition.). At the end of flaming combustion, large amounts of residue were observed; their surface glowed under the continuous external radiant heat flux of  $50 \text{ kW/m}^2$  and the residues were consumed in conjunction with the smoldering. The residues were collected after two minutes continuous exposure to the external flux beyond the end of flaming combustion; pictures of these are shown in Fig. 4. PP did not leave any residue, PP/MWNT(2%) left mainly an orange/red color residue, and PP/MWNT(4%) left a mixed residue consisting of orange/red color material and a black ‘flocule’.

An EDS analysis of the residues was conducted and the results are shown in Fig. 5. The results for the orange/red color residue show large peaks for Fe and O (the Si peak is due to a silicon substrate) with a small peak at C. This indicates that the orange/red residue mainly consists of iron oxide, which was formed from oxidation of residual iron particles. However, the results of the black floccule show a peak at C with a small peak of O. Thus, the floccule residue mainly consists of carbon nanotubes (because X-ray diffraction of the residue shows sharp peaks at  $2\theta$  of  $26.1^\circ$  corresponding (002) peak, at  $2\theta$  of  $43.3^\circ$  corresponding (100) peak, and at  $2\theta$  of  $53.3^\circ$  corresponding (004) peak of graphite and MWNTs did degrade only 2.9% at  $1600^\circ\text{C}$  [28] which is well over the temperature range of the sample (roughly  $400\text{--}500^\circ\text{C}$ ) during the flaming period (no oxygen to the burning surface) in a cone calorimeter) and some

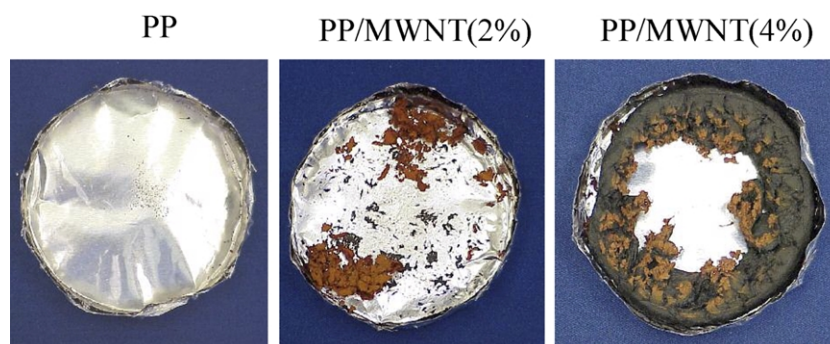
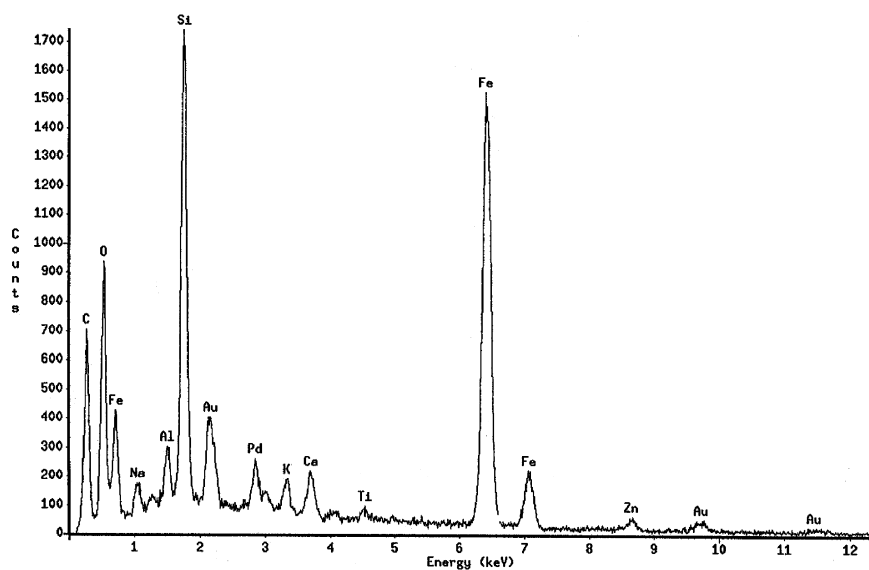
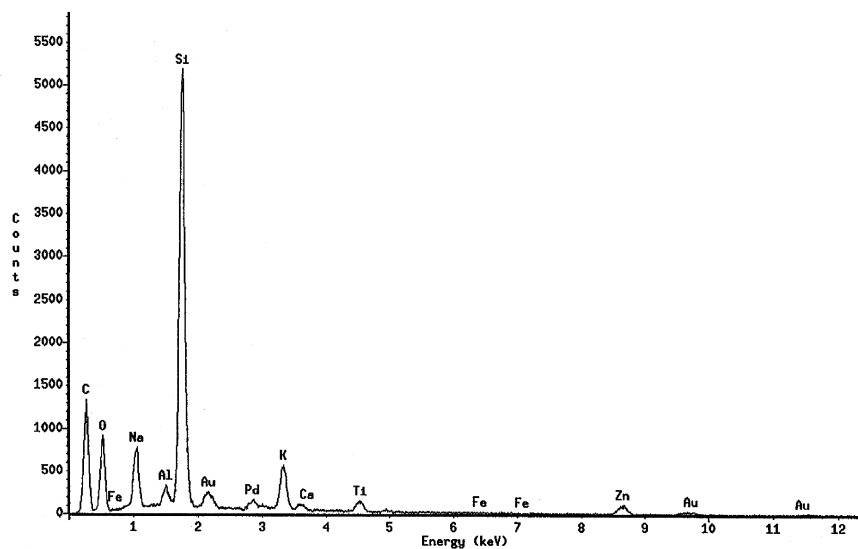


Fig. 4. Collected residues after the Cone Calorimeter test (in air) with additional 2 min heating after flame out at  $50 \text{ kW/m}^2$  (showing the effects of consumption of the residue by smoldering).



(a)



(b)

Fig. 5. EDS spectra of the collected residues after tests in Cone Calorimeter, (a) red/orange residue and (b) black floccule residue.

of tubes appeared to be partially oxidized. The carbon nanotubes in the residue of PP/MWNT(2%) were nearly completely consumed by smoldering during the two minutes exposure period but some of them survived in the residue of PP/MWNT(4%). The iron oxides in the residue whose analysis is shown in Fig. 5 were more or less crumpled and not well dispersed in the overall residue. The temperature of the smoldering residue surface is estimated to be as high as 900 °C which is well below the melting temperature of iron. It is not clear how the observed distribution of the iron oxides in the residue was formed.

### 3.3. Effects of MWNT concentration on flammability properties

The quantity of MWNTs in PP was varied up to 4% by mass fraction; the measured heat release rate curve for each sample is shown in Fig. 6 for comparison. The results show two distinct characteristics brought on by the addition of MWNTs; first, there is a shortened ignition delay time with the PP/MWNT(0.5%) followed by an increased ignition delay time with an increase in the concentration of MWNT; second, there is a gradual increase in peak heat release rate above about 1% by mass of MWNT. The TGA data of

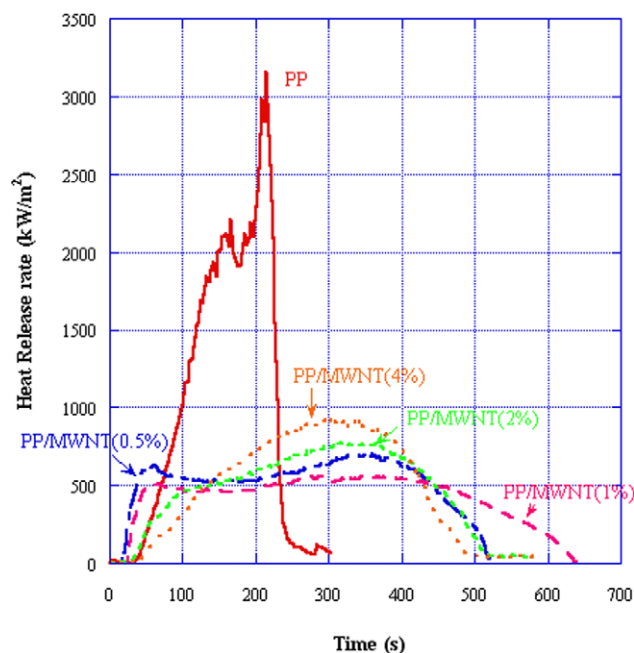


Fig. 6. Effects of concentration of MWNT in PP on heat release rate of PP/MWNT nanocomposite at  $50 \text{ kW/m}^2$ .

PP/MWNT(2%) and PP/MWNT(4%) show a slight increase in thermal stability compared to that of PP, both in nitrogen and in air [21]. This TGA stability trend would be expected to somewhat increase the ignition delay time but it does not agree with the trend of ignition delay time observed in Fig. 6. In the cone calorimeter test, ignition is initiated by thermal radiation from an electrically heated element at a temperature of about  $750^\circ\text{C}$ . It is expected that the emission spectra from the heater element is that of a gray body covering from the visible to the far infrared but peaking at about  $2.7 \mu\text{m}$ . Therefore, there might be significant

difference in absorption characteristics of the external emission by PP/MWNT as compared to that of PP. The measured infrared transmission spectra of the PP sample was compared with that of the PP/MWNT(1%) nanocomposite; see Fig. 7. The PP shows many absorption bands based on various vibrational modes but substantial transmission between them. This indicates that the external thermal radiant flux of  $50 \text{ kW/m}^2$  is absorbed by the PP sample over some depth. On the other hand, the PP/MWNT nanocomposite shows no significant transmission bands and all of the  $50 \text{ kW/m}^2$  flux is absorbed very near the sample surface, within a distance of  $200 \mu\text{m}$ . Therefore, a narrow layer in the vicinity of the PP/MWNT sample surface is rapidly heated and its temperature becomes high enough to initiate thermal degradation of PP and to generate evolved degradation products of monomer dimer, trimer, and others to initiate ignition. On the other hand, the PP sample is heated over a greater depth and it thereby takes a longer time to heat the sample to initiate degradation. Thus, the ignition delay time of PP/MWNT, in particular at low concentration of MWNT, tends to be shorter than that of PP.

The subsequent trend of an increase in ignition delay time with an increase in the concentration of MWNT could have the same origin as the increased peak heat release rate with an increase in the concentration of MWNT above 1% by mass. It has been shown that the thermal conductivity of a single MWNT is more than  $3000 \text{ W/mK}$  at room temperature [32] and that of the microscopic mat MWNT sample is about  $20 \text{ W/mK}$  [33]. It is postulated that the observed MWNT distribution shown in Figs. 1 and 2 indicates that the thermal conductivity of the MWNT structure in PP might be as high as the previously published value ( $20 \text{ W/mK}$ ). It thus is possible that the thermal conductivity of the PP/MWNT nanocomposite would increase appreciably with an increase in the concentration of MWNT in PP. With this assumption, the qualitative effects of an increase in thermal conductivity on the trend of the mass loss rate curve of PP (without carbon nanotubes) under an external heat flux of  $50 \text{ kW/m}^2$  in nitrogen (without any flaming combustion) were estimated by numerically solving a one dimensional transient differential energy equation with one step, first order degradation kinetics in depth. The external heat flux was assumed to be absorbed at the sample surface and the degradation products were evolved to the gas phase instantly (no in-depth transport resistance). The back surface of the sample was assumed to be thermally insulated. In the calculation, thermal conductivity was assumed to be constant with respect to temperature but varied from that of PP alone to two times that of the PP value. The results are shown in Fig. 8 and show two distinct trends with an increase in thermal conductivity; one is the reduction of the initial mass loss rate and the other is an increase in the mass loss rate late in the test. An increase in thermal conductivity increases thermal conduction from the high temperature sample surface to the interior of the sample and thereby delays the onset of sample

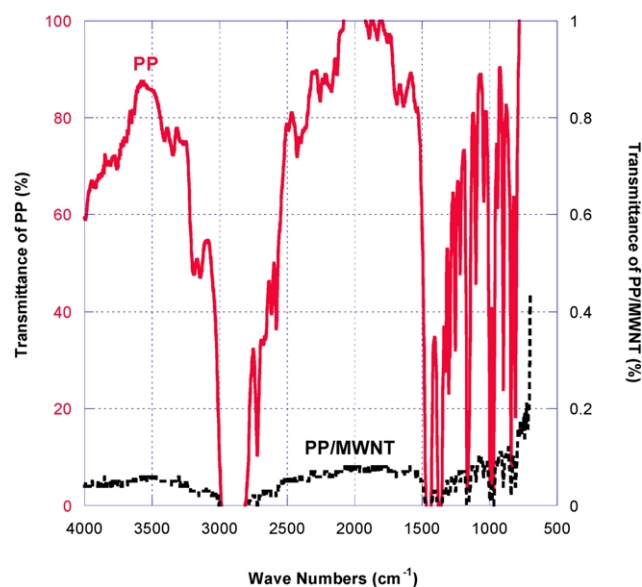


Fig. 7. Comparison of transmission spectra between PP and PP/MWNT(1%) through  $200 \mu\text{m}$  thick film.

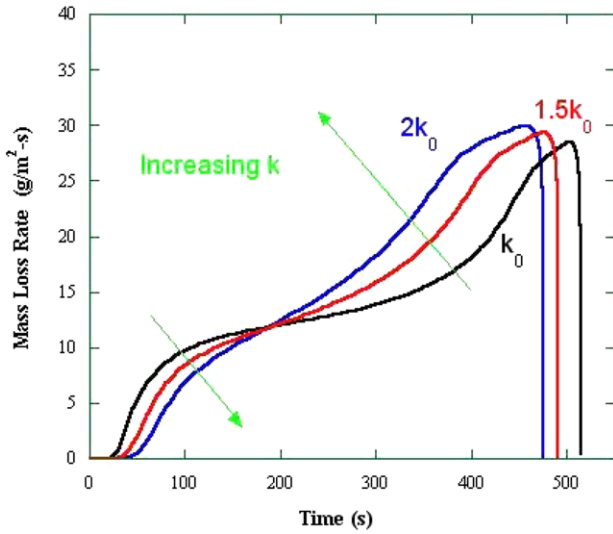


Fig. 8. Calculated effects of an increase in thermal conductivity on mass loss rate of PP at 50 kW/m<sup>2</sup> in nitrogen.

mass loss (delays ignition). Since the backside of the sample surface is thermally insulated, the increase in thermal conduction from the heated sample surface enhances the accumulation of heat in the virgin sample and the sample temperature near the backside surface increases. Thus, the peak mass loss rate near the final consumption of the sample increases with an increase in thermal conductivity.

Thermal conductivities of the PP sample and the PP/MWNT nanocomposite were measured as a function of temperature to confirm the assumption that the thermal conductivity of the nanocomposite is higher than that of the PP sample. The results are shown in Fig. 9. We conducted the measurements as follows: (1) the sample was heated to

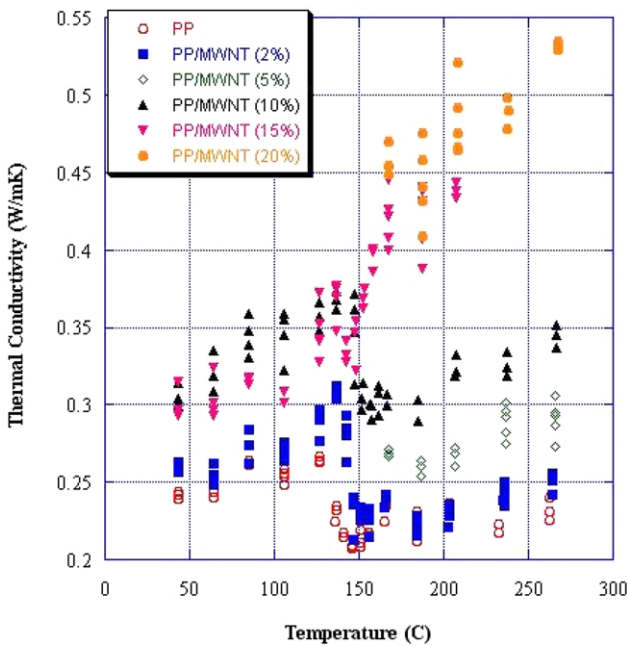


Fig. 9. Comparison of thermal conductivity between PP and PP/MWNT nanocomposite.

200 °C; (2) the sample was then slowly cooled and measurements were conducted at decrements of about 20 °C down to 160 °C; (3) the measurement was conducted at a decrement of 5 °C from 160 to 130 °C; (4) the measurement was conducted at decrements of about 20 °C down to 40 °C; and (5) then the sample was heated to 200 °C and the measurement was conducted at an increment of about 30–260 °C. If we conducted the measurement at a decrement of 20 °C from 200 °C down to 40 °C, the data below 160 °C show a monotonic decrease with a decrease in temperature instead of the results shown in Fig. 9. This difference appears to be caused by less formation of crystallites in PP due to rapid cooling with a 20 °C decrement between measurements through the melting regime. Previously published results indicate that thermal conductivity of PP is higher below the melting than above melting due to the formation of crystals [25,34]. We obtained a similar trend with the slow cooling experiment using the 5 °C decrement between measurements. The thermal conductivity of PP/MWNT increases with an increase in the amount of MWNT and the effects of the formation of crystals can be seen up to 10% of MWNT by mass. However, the thermal conductivities of PP/MWNT samples with 15 and 20% of MWNT by mass increase monotonically with an increase in temperature. This trend could be due to reduction of crystallization because of the large surface area and extended shape of the MWNTs. The thermal conductivities of the two PP/MWNT samples become much higher than the samples with lower amount of MWNT above 160 °C. However, the increase in thermal conductivity appears rather limited by the exceptionally small interface for thermal conductance compared to that in electric conductivity [35]. When the PP/MWNT(1%) sample was burning, PP in the sample gradually receded leaving MWNTs behind as described in the Section 3.4.3. During this process, the concentration of MWNT in the sample increases from the original 1% by mass to, eventually 100% by mass. The network layer mainly consisting of MWNTs without the PP component is porous for the nanocomposite with 1% mass of MWNT due to roping of tubes caused by the gasification of PP, as shown in Fig. 15. The measured increase in thermal conductivity of PP/MWNT (5%) is roughly 30% above that of pure PP compared to one and half or two times used in the numerical calculation, as shown in Fig. 8. However, the model calculation is highly idealized and does not include indepth absorption of incident radiant flux and MWNTs (the formation of network consisting of MWNTs shields the external radiation as discussed later); it is intended to show a qualitative trend of the effects of an increase in thermal conductivity on mass loss rate of PP (the reduction of the initial mass loss rate and an increase in the mass loss rate late in the test). Thus, we infer that the above described trends, longer ignition delay time and higher peak heat release rate by increasing the concentration of MWNT in

PP, are mainly due to an increase in thermal conductivity of PP/MWNT.

### 3.4. Flame retardant mechanism of PP/MWNT nanocomposites

#### 3.4.1. Flame retardant action site

Flame retardant action can be attributed to two possible domains or a combination: in the gas phase, in the condensed phase, and in both phases simultaneously. As described in Section 2, the results obtained in the radiative gasification device in a nitrogen atmosphere are purely based on the chemical and physical processes in the condensed phase. If the results obtained in a cone calorimeter (with combustion) are very similar to those obtained in the gasification device, the observed improvement in flammability properties is mainly based on the processes in the condensed phase. If the cone calorimeter shows much better results (less heat release or lower mass loss rate) than the results obtained in the gasification device, the flame retardant action is mainly based in the gas phase. An example of the latter is a conventional brominated flame retardant.

The mass loss rate curves of PP, PP/MWNT(0.5%), and PP/MWNT(1%) obtained in the cone calorimeter are compared with those obtained in the nitrogen gasification device, as shown in Fig. 10. Since there is additional heat feedback from the flame to the sample surface in the cone

calorimeter, mass loss rates obtained in the cone calorimeter are larger than those obtained in the gasification device (no flaming). The comparison shows roughly 25% larger mass loss rates in the cone calorimeter than those in the gasification device and thus the samples were consumed much quicker in the cone calorimeter than in the gasification device. The difference in mass loss rate among the three samples in the cone calorimeter is very similar to that in the gasification device. This trend and the constancy of the averaged specific heat of combustion (measured heat release rate divided by mass loss rate) for all samples ( $43 \pm 2$  MJ/kg) clearly indicate that the observed flame retardant performance of the PP/MWNT nanocomposite is mainly due to chemical or/and physical processes in the condensed phase. These results also indicate that the PP/MWNT nanocomposites burn slower than PP but they all burn nearly completely. These observations are similar to those with clay nanocomposites [5,6].

The physical behavior of the PP/MWNT nanocomposites was significantly different from that of PP during the gasification test. As shown in Fig. 11(a), the PP sample behaved like a liquid with fine froth layer generated by the bursting of numerous small bubbles at the sample surface. No char was left at the end of the test. However, all PP/MWNT samples tested in this study behaved like a solid without any visible melting except at the very beginning of the test and the shape or size of the sample did not change significantly during the test. Only a slight shrinkage was

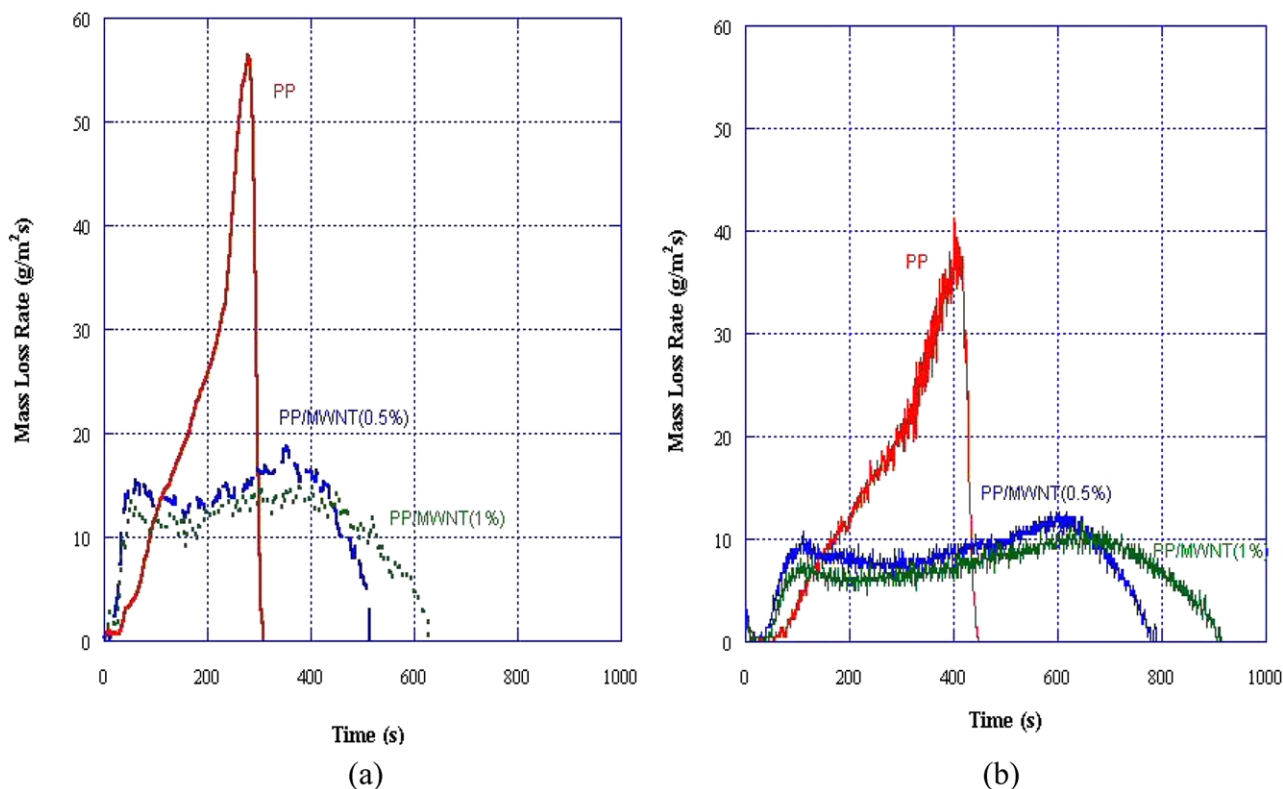


Fig. 10. Effects of MWNT addition on mass loss rate of PP at external flux of  $50 \text{ kW/m}^2$ , (a) burning in the Cone calorimeter, (b) no-flaming mass loss rate in nitrogen in the gasification device.

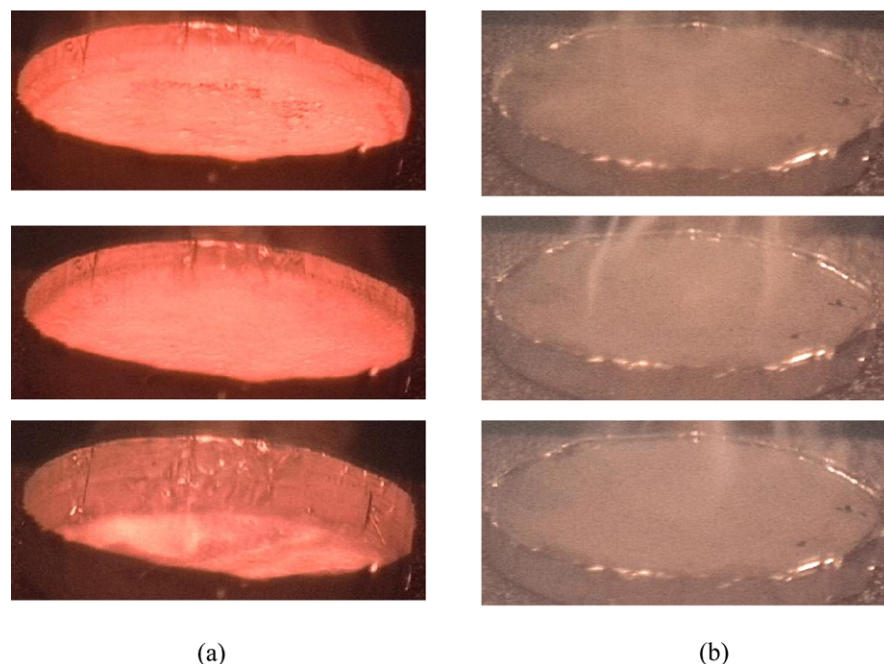


Fig. 11. Sample behavior in the gasification test at  $50 \text{ kW/m}^2$  in nitrogen, (a) PP, and (b) PP/MWNT(1%).

observed. A light network of floccules was left at the end of the test; a more detailed discussion of the floccules is given in Section 3.4.3.

#### 3.4.2. MWNT vs carbon black

Since carbon black has been used as a filler to enhance physical properties of rubbers, the observed flame retardant performance could be due to the addition of carbon alone independent of its size or/and shape. In order to test this hypothesis, two different carbon blacks having different

surface areas were compounded with PP at the same level of carbon concentration in PP as those of the PP/MWNT nanocomposites. The surface area of the carbon black designated as N299 was  $102 \text{ m}^2/\text{g}$  and that designated as N762 was  $27.3 \text{ m}^2/\text{g}$ . Since the flame retardancy active site is mainly in the condensed phase, as discussed in the previous section, mass loss rate curves of the PP/carbon black samples were measured in the gasification device in a nitrogen atmosphere and the sample residues were collected at the end of tests. The mass loss rate curves of the PP/carbon black samples are compared with that of PP in Fig. 12. The addition of either carbon black increased the initial mass loss rate compared to that of PP. This trend is similar to the addition of MWNTs to PP as shown in Fig. 10(b) but the reduction in the peak mass loss rate is not nearly as great compared to that for the PP/MWNT nanocomposites. The initial increase in mass loss rate for the PP/CB samples is due to an increase in the absorption coefficient for the incident radiation due to the addition of carbon black, similar to that with MWNTs, as described in Section 3.3. During the gasification test with the PP/CB samples, the sample appeared to be a viscous liquid with the formation of large bubbles, which frequently burst at the sample surface. These results indicate that the flame retardant effectiveness of the PP/MWNT nanocomposites is mainly due to extended shape of the MWNTs. The next section clearly shows the effects of the shape of carbon particles on the formation of the sample residue.

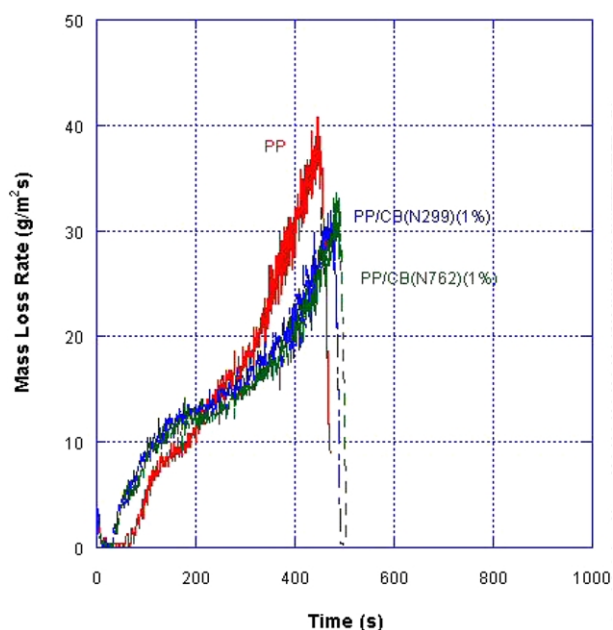
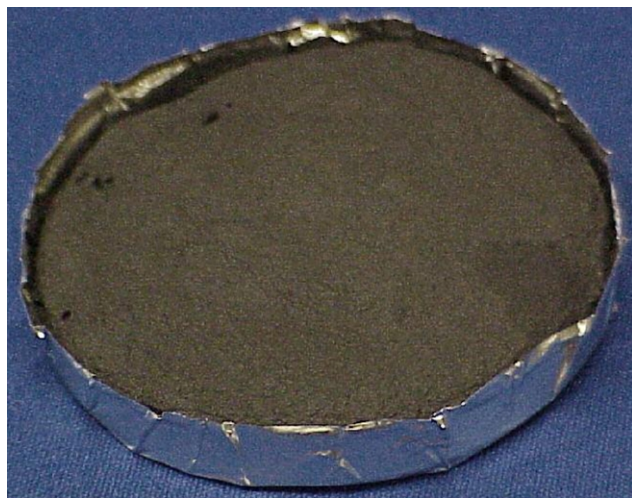


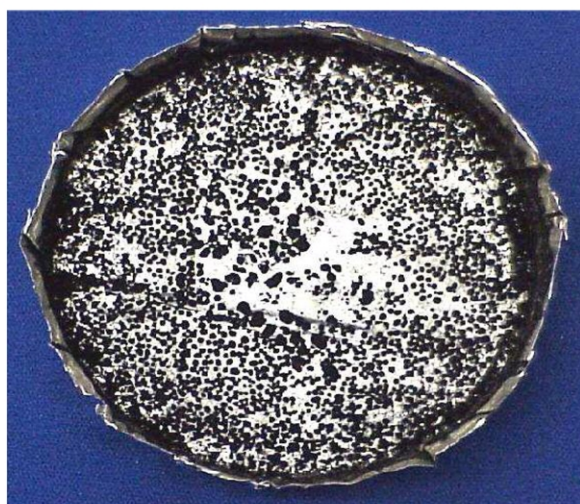
Fig. 12. The effects of addition of carbon black on mass loss rate of PP at  $50 \text{ kW/m}^2$  in nitrogen.

#### 3.4.3. Sample residues

The residue of each sample tested in the gasification device at  $50 \text{ kW/m}^2$  in a nitrogen atmosphere was collected after the test. The pictures of the residue of the



(a)



(b)

Fig. 13. Collected residues after the gasification experiment at  $50 \text{ kW/m}^2$  in nitrogen. (a) PP/MWNT(1%) and (b) PP/CB(N299)(1%).

PP/MWNT(1%) nanocomposite and of the PP/CB(1%) are shown in Fig. 13. The shape of the residue of the PP/MWNT(1%) is nearly the same as the original sample except for slight shrinkage. No cracks were observed in any residue of

the PP/MWNT nanocomposites. However, both residues of the PP/CB samples consisted of dispersed, aggregated granular particles left at the bottom of the sample container. Careful observation shows that granular particles accumulated more around the periphery of the sample container. The particles could be pushed toward the periphery by the numerous rising bubbles and their associated convective motions in the molten sample; the particles did not form a network structure to cover the sample surface and thereby protect/shield virgin sample. The networked layer of the PP/MWNT samples cover the entire sample surface and extends to the bottom of the residue as shown in Fig. 14. The residue consists of tangled and stacked carbon nanotubes, as shown in Fig. 15 and in our previous paper [21]. The tubes in the residue are more 'intertwined' and larger than those in the original sample. The network layer is porous but has physical integrity and does not break when lightly picked at by one's fingers. The mass of the network layer is very close to the initial mass of carbon nanotubes in the original nanocomposite. This indicates that the networked layer does not enhance char formation from PP.

The thermal characteristics of the networked layer are important in determining the flame retardant effectiveness of the PP/MWNT nanocomposites. Tests were conducted to measure the transmission of a broadband external radiant flux and also the thermal insulation performance of the residual floccule layer. (In order to obtain residues having different thicknesses, PP/MWNT samples with two additional thicknesses of 1.6 and 4 mm were prepared by compression molding. These new samples were tested at  $50 \text{ kW/m}^2$  in nitrogen and residues were collected after the end of the tests.) A schematic illustration of the experimental set-up is shown in Fig. 16. The test was conducted in the gasification device in a nitrogen atmosphere to avoid any exothermic glowing combustion of the floccule layer in air. At first, the external radiant heat source was turned on with the closed water cooled shutter over the residue until the heat source reached a steady temperature emitting a steady flux of about  $51 \text{ kW/m}^2$ . Then, the shutter was opened by a pneumatic piston and the residual floccule layer was exposed to the external radiant flux. The layer was directly mounted on (and in contact with) a water cooled Gardon type flux gauge (diameter of 15 mm), which recorded heat

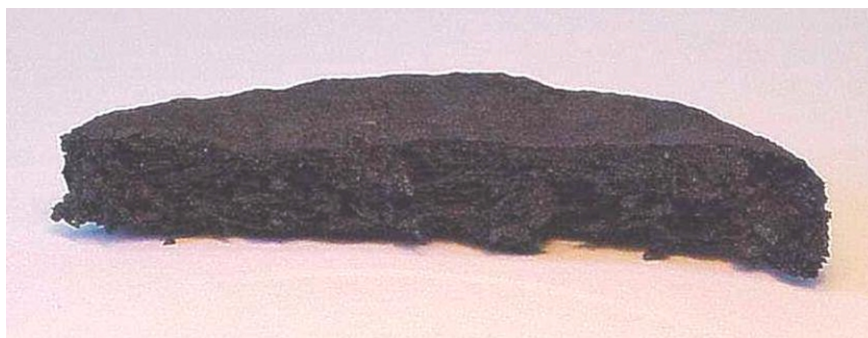


Fig. 14. The cross section of the residue of the PP/MWNT(1%) nanocomposite shown in Fig. 13(a).

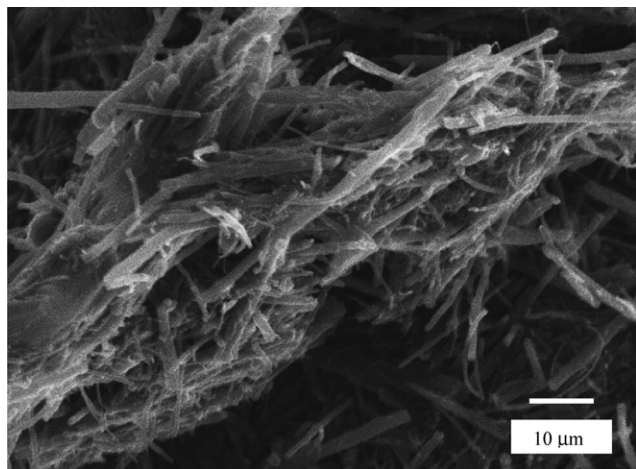


Fig. 15. SEM picture of the floccule residue of PP/MWNT(4%) which was collected after the Cone Calorimeter test at  $50 \text{ kW/m}^2$ .

flux through the layer. The recorded transmitted fluxes through the residual floccule layers of the various PP/MWNT samples are shown in Fig. 17. Note that since the sample heats up (at least on its uppermost layers), the flux gage sees a combination of pure transmission plus a part of re-emission from the hot layers. The results show that the gage detected the steady-state values of transmitted flux nearly instantly within 2–3 s from the start of opening of the shutter, (full opening took about 1 s, the response of the gage was about 1 s, and data were taken every 1 s). The transmitted flux decreases strongly with the thickness of the nanotube network layer and weakly with an increase in the concentration of MWNT in the original sample. Another important aspect of the results is that the transmitted flux remained constant during a 6 min period even with a thin 1.6 mm thick residue of PP/MWNT(1%). This means that thermal conduction through the network layer appears to be negligible compared to radiative transfer. The layer is porous but spectroscopically opaque (nearly a blackbody as shown in Fig. 7). The heat balance through the residue reaches a steady state very quickly. The external radiant flux of  $50 \text{ kW/m}^2$  was absorbed at the top layer of the residue and heated the layer nearly instantaneously due to its low

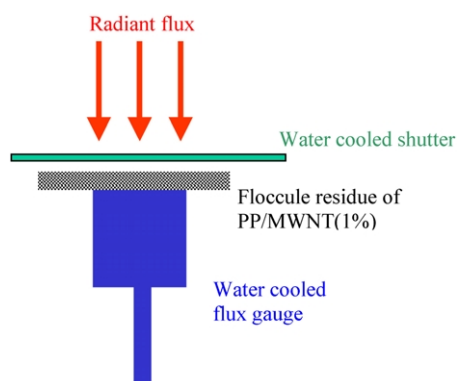


Fig. 16. Schematic illustration of characterization test of the collected floccule residue of PP/MWNT(1%) in nitrogen.

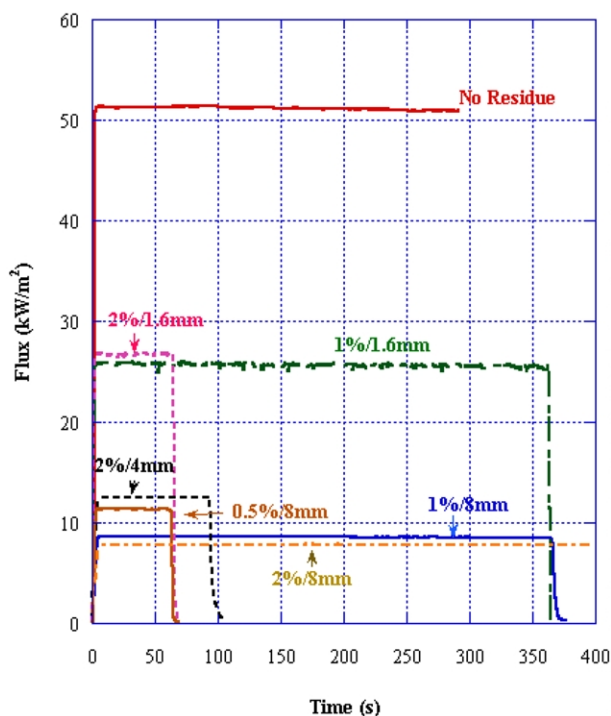


Fig. 17. Transmission characteristics of the floccule residue of PP/MWNT(1%) collected from the gasification test at  $50 \text{ kW/m}^2$  in nitrogen. (Since flux does not change with time, some of the measurements were terminated at shorter times.)

density (about  $0.02 \text{ g/cm}^3$  for the residue of PP/MWNT(1%)). The hot top layer re-emitted radiation to the gas phase as a heat loss and also to the inside of the residue. Since the heat up time of the floccule was nearly instantaneous due to its low density, achievement of steady-state radiative transfer through the residue was very quick. Using the specific heat value of  $1000 \text{ J/kg K}$  for MWNT [36], the estimated energy need to heat the residue of 1.6 mm to  $500^\circ\text{C}$  was about 6% of the energy absorbed by the residue at the incident flux of  $51 \text{ kW/m}^2$ . The rest of the absorbed energy was lost from the irradiated surface and also from the backside surface of the residue. The transmitted flux (radiative and conductive) of about  $25 \text{ kW/m}^2$  from the backside surface (about 50% of the incident flux) is shown in Fig. 17. Since the temperature of the gage was close to the cold coolant water temperature, the heat loss from the backside sample could be larger than that from the irradiated surface due to additional conductive loss to the gage (convective loss caused by buoyancy from the irradiated, hot surface tends to be much smaller than radiative loss). If the heat loss from the irradiated surface is estimated by the difference from the incident flux minus the flux loss from the backside surface and the energy to heat the residue, then it is about  $22 \text{ kW/m}^2$  which corresponds to about  $520^\circ\text{C}$  with an assumed emissivity of 1. This examination of the energy balance through the nanotube network layer shows that it acts as a thermal shield to reduce the exposure of the polymer resin in the nanocomposite to

an external radiant flux or to heat feedback from a flame. Since the PP/MWNT(1%) is nearly opaque as discussed above (also its residue assumed to be spectroscopically opaque), additional MWNT in the floccule residue does not modify radiative transfer through the residue except that it increases the latent energy to heat the additional mass; this is relatively small compared to radiative flux. This probably is the reason why the higher MWNT concentration in PP/MWNT used in this study does not have significantly greater effects on the transmitted flux through the nanotube network residue.

The condensed phase process during the burning of the PP/MWNT nanocomposite can be summarized as follows. After the start of irradiation by the external radiant flux on the PP/MWNT nanocomposite surface, the temperature near the sample surface increases with time. When the sample temperature reaches the degradation temperature range of the PP (350–450 °C), the PP in the PP/MWNT nanocomposite sample degrades and its uppermost surface gradually regresses below the original surface position, now marked by the top of the MWNT network layer. MWNTs are thermally stable so the original network structure of MWNTs stays almost in place as they were in the nanocomposite sample except for some ‘roping’ caused during gasification of PP. The temperature of the thin network layer increases significantly due to its opaqueness and low density; thermal emission from this high temperature network layer enhances heat loss to the gas phase (the temperature of the sub-layer containing significant amounts of PP remains in the range of its degradation temperature due to its overall endothermic degradation). More heat is transferred to the interior of the sample. With an increase in exposure time to the external radiant flux, the PP upper surface layer recedes deeper into the nanocomposite sample and the nanotube layer becomes thicker. The heat transfer mode through the thicker nanotube network layer is presumably radiative transfer instead of thermal conduction. Close to 50% of the incident flux is lost by the emission from the hot nanotube surface layer and the remainder of the flux is transferred to the nanotube network layer and the virgin sample. Therefore, the role of the nanotube network layer appears to be a radiation emitter from the surface consequently to act as a radiation shield. The layer appears not to be a barrier for degradation products (no cracks or swelling were observed) with the MWNT contents used in this study. Due to accumulation of the heat in the virgin sample (the backside sample was thermally insulated in the experiment), the heat release rate increases with higher contents of MWNT in the sample, as shown in Fig. 6. The nanotube network layer becomes more dense for the samples with higher contents of MWNT. However, heat transfer through the nanotube network layer does not change (it is still nearly opaque) until the content of MWNT is so high that a heat conduction mode through the MWNTs themselves becomes significant.

The floccule network layer is most effective for reducing

flammability if it covers the entire sample surface without any significant cracks. This is achieved by forming the networked floccule structure, which has physical integrity without breaking during burning. Its structure is porous enough so that the layer appears not to act as a barrier for degradation products of PP. It is possible that some molten PP inside the nanocomposite sample could be transported to the sample surface by capillary action through the nanotube network layer. A protective layer was also observed with PP/clay nanocomposites, but the layer was brittle and it required a minimum of 5% by mass of clay particles in PP to form a layer which covered the entire sample surface [37]. Furthermore, polypropylene-graft-maleic anhydride (PP-g-MA) was needed as a compatibilizer between the hydrophilic clay and the hydrophobic PP to make the nanocomposite instead of a microcomposite. PP-g-MA formed a small amount of char, which was needed to strengthen the protective layer formed from the clay particles. Since the PP/MWNT nanocomposites used in this study do not need any compatibilizer and required only about 1% by mass in PP, it appears that the PP/MWNT nanocomposite is a more effective flame retardant sample than the PP/clay nanocomposite.

#### 4. Conclusions

The thermal and flammability properties of PP/MWNT nanocomposites were measured. The thermal conductivity of the nanocomposite increases with an increase in MWNT content in particular above 160 °C, but does not increase nearly as dramatically as the increase in electric conductivity. Since the radiant flux absorptivity at infrared wavelengths increases significantly with the addition of MWNTs to PP, the radiative ignition delay time of the PP/MWNT (0.5%) nanocomposite is less than that of PP. Ignition delay time and the peak heat release rate of the PP/MWNT increase with the MWNT content in the nanocomposite above 1% by mass. The lowest heat release rate is observed with the PP/MWNT(1%) sample due to the balance between the effect of thermal conductivity and the shielding performance of external radiant flux (and heat feedback from the flame) depending on the concentration of MWNT in the sample. A nanotube network layer consisting of carbon nanotubes is formed and it covers the entire sample surface without any significant cracks forming during burning. The PP/CB sample does not form the nanotube network layer and its heat release rate is not significantly different from that of PP. The hot surface of the nanotube network layer loses a significant amount of heat flux by emission to the gas phase and shields external radiant flux reducing transmitted flux to receding PP in the sample. The effects of residual iron particles and defects in the MWNTs on flammability performance of the PP/MWNT nanocomposites are negligible.

## Acknowledgements

The authors would like to thank Dr Richard Davis for compounding PP with carbon black particles, Mr Michael Smith for some of the Cone Calorimeter measurements, Mr Kaoru Wakatsuki for the IR transmission measurement, and Dr Thomas Ohlemiller for valuable discussions on the flammability mechanism of the nanocomposites.

## References

- [1] Kojima Y, Usuki A, Kawasumi M, Okada A, Fukushima Y, Kurauchi T, Kamigaito O. *J Mater Res* 1993;8:1185–9.
- [2] Giannelis EP. *Adv Mater* 1996;8:29–35.
- [3] Wang Z, Pinnavaia TJ. *Chem Mater* 1998;10:1820–6.
- [4] Kashiwagi T, Shields JR, Harris Jr RH, Davis RD. *J Appl Polym Sci* 2003;87:1541–53.
- [5] Gilman JW, Kashiwagi T. *SAMPE J* 1997;33:40–6.
- [6] Gilman JW. *Appl Clay Sci* 1999;15:31–49.
- [7] Gilman JW, Jackson CL, Morgan AB, Harris Jr R, Manias E, Giannelis EP, Wuthenow M, Hilton D, Phillips SH. *Chem Mater* 2000;12:1866–73.
- [8] Zanetti M, Camino G, Mülhaupt R. *Polym Degrad Stab* 2001;74:413–7.
- [9] Zhu J, Uhl FM, Morgan AB, Wilkie CA. *Chem Mater* 2001;13:4649–54.
- [10] Alexandre M, Beyer G, Henrist C, Cloots R, Rulmont A, Jerome R, Dubois P. *Macromol Rapid Commun* 2001;22:943–6.
- [11] Zhu J, Start P, Mauritz A, Wilkie CA. *Polym Degrad Stab* 2002;77:253–8.
- [12] Morgan AB, Harris Jr RH, Kashiwagi T, Chyall LJ, Gilman JW. *Fire Mater* 2002;26:247–53.
- [13] Kashiwagi T, Harris RH Jr, Zhang X, Briber RM, Cipriano BH, Raghavan SR, Awad WH, Shields JR. *Polymer* 2004;45:881–91.
- [14] Shaffer MSP, Windle AH. *Adv Mater* 1999;11:937–41.
- [15] Qian D, Dickey EC, Andrews R, Rantell T. *Appl Phys Lett* 2000;76:2868–71.
- [16] Jin Z, Pramoda KP, Xu G, Goh SH. *Chem Phys Lett* 2001;337:43–7.
- [17] Thostenson ET, Chou TW. *J Phys D: Appl Phys* 2002;35:L77–L80.
- [18] Bin Y, Kitanaka M, Zhu D, Matsuo M. *Macromolecules* 2003;36:6213–9.
- [19] Pötschke P, Dudkin SM, Alig I. *Polymer* 2003;44:5023–30.
- [20] Safadi B, Andrews R, Grulke EA. *J Appl Polym Sci* 2002;84:2660–9.
- [21] Kashiwagi T, Grulke E, Hilding J, Harris Jr RH, Awad WH, Douglis J. *Macromol Rapid Commun* 2002;23:761–5.
- [22] Beyer G. *Fire Mater* 2002;26:291–3.
- [23] Kashiwagi T, Du F, Winey KL, Harris RH Jr, Shields JR, Douglas JF. Submitted publication.
- [24] Andrews R, Jacques D, Rao AM, Derbyshire F, Qian D, Fan X, Dickey EC, Chen J. *Chem Phys Lett* 1999;303:467.
- [25] Lobo H, Cohen C. *Polym Engng Sci* 1990;30:65–70.
- [26] Austin PJ, Buch RR, Kashiwagi T. *Fire Mater* 1998;22:221–37.
- [27] Lee CJ, Park J, Huh Y, Lee JY. *Chem Phys Lett* 2001;343:33–8.
- [28] Bom D, Andrews R, Jacques D, Anthony J, Chen B, Meier MS, Selegue JP. *Nano Lett* 2002;2(6):615–9.
- [29] Andrews R, Jacques D, Qian D, Dickey EC. *Carbon* 2001;39:1681–7.
- [30] Hirschler MM. *Polymer* 1984;25:405.
- [31] Carty P, White S. *Fire Safety J* 1994;23:67.
- [32] Kim P, Shi L, Majumdar A, McEuen PL. *Phys Rev Lett* 2001;87:215502.
- [33] Yi W, Lu L, Zhang DL, Pan ZW, Xie SS. *Phys Rev B* 1999;59:R9015–8.
- [34] Zhang X, Hendro W, Fujii M, Tomimura T, Imaishi N. Presented at the 14th Symposium on Thermophysical Properties, Boulder, Co, USA; June 2000.
- [35] Hutable ST, Cahill DG, Shenogin S, Xue L, Ozisik R, Barone P, Usrey M, Strano MS, Siddons G, Shim M, Keblinski P. *Nature Mater* 2003;2:731.
- [36] Yi W, Lu L, Zhang DL, Pan ZW, Xie SS. *Phys Rev B* 1999;59:PRB59.
- [37] Morgan AB, Kashiwagi T, Harris RH, Campbell JR, Shibayama K, Iwasa K, Gilman JW. In: Nelson GL, Wilkie CA, editors. *Fire and polymers*. ACS Symposium Series 797; 2001. Chapter 2.